Astron. Astrophys. 356, 501–516 (2000)

ASTRONOMY AND ASTROPHYSICS

Infrared imaging and spectroscopy of the Luminous Blue Variables Wra 751 and AG Car⋆⋆⋆

R.H.M. Voors[1,2,3], L.B.F.M. Waters[3,4], A. de Koter[3], J. Bouwman[3], P.W. Morris[1,3], M.J. Barlow[5], R.J. Sylvester[5], N.R. Trams[6], and H.J.G.L.M. Lamers[2,1]

[1] SRON Laboratory for Space Research, Sorbonnelaan 2, 3584 CA Utrecht, The Netherlands
[2] University of Utrecht, Astronomical Institute, Princetonplein 5, 3584 CC Utrecht, The Netherlands
[3] University of Amsterdam, Astronomical Institute Anton Pannekoek, Kruislaan 403, 1098 SJ Amsterdam, The Netherlands
[4] Katholieke Universiteit Leuven, Instituut voor Sterrenkunde, Celestijnenlaan 200B, 3001 Heverlee, Belgium
[5] University College London, Department of Physics and Astronomy, Gower St., London WC1E 6BT, UK
[6] Integral Science Operations, Astrophysics Division of ESA, ESTEC SCI-SAG, PO Box 299, 2200 AG Noordwijk, The Netherlands

Received 10 March 1999 / Accepted 10 January 2000

Abstract. We present ground-based infrared imaging and ISO spectroscopy of the luminous blue variables Wra 751 and AG Car. The images show in both cases a detached shell with a roughly circular distribution of emission. The infrared images of AG Car coincide very well with the optical images. The optical (Hα) image of Wra 751 is different from the infrared image; the Hα nebula is suggested to be a scattering nebula containing cold dust particles.

Fitting both the images and the spectra consistently with a 1-D radiative transfer model, we derive properties of their dust shells. Wra 751 is surrounded by a dust shell with inner and outer radii of 0.17 and 0.34 pc respectively and a dust mass of 0.017 $M_\odot$. The dust shell of AG Car has inner and outer radii of 0.37 and 0.81 pc respectively and a total dust mass of 0.25 $M_\odot$. Dust mass-loss rates during the formation of the shells are 2.7×10^{-6} and 3.4×10^{-5} $M_\odot$ yr^{-1}, respectively. The total dust mass and hence the derived dust mass-loss rates are uncertain by at least a factor of two. For AG Car, the derived dust mass and mass-loss rate are higher than previous estimates. This is mainly caused by the fact that a contribution of very large grains (> 10 μm) is needed to explain the flux levels at longer wavelengths.

Dust models for both objects fail to explain the flux shortward of 15 to 20 μm: a population of small warm grains, not in thermal equilibrium with the central star is necessary to explain this excess. Similarities between dust shells around Wolf-Rayet stars and Wra 751 and AG Car (mass, grain size population, morphology) suggest a similar formation history and imply an evolutionary connection. A similar connection with red supergiants is suggested on the basis of the dust composition and derived time-averaged mass-loss rates.

Send offprint requests to: L.B.F.M. Waters: rensw@astro.uva.nl

⋆ based on observations obtained with ISO, an ESA project with instruments funded by ESA Member states (especially the PI countries: France, Germany, the Netherlands and the United Kingdom) with the participation of ISAS and NASA

⋆⋆ based on observations obtained at ESO, La Silla, Chile

Key words: stars: circumstellar matter – stars: evolution – stars: individual: Wra 751, AG Car – stars: mass-loss

1. Introduction

The class of Luminous Blue Variables (LBVs) consists of a small number of very massive, hot unstable stars in the upper left part of the HR diagram. LBVs are characterised by very high present-day mass-loss rates ($\sim10^{-5}$ $M_\odot$ yr^{-1}) via an ionized wind, expanding at modest velocities (100 to 500 km s^{-1}). One of the defining criteria for LBVs is their variability, on various time-scales and amplitudes. All LBVs show small amplitude variability on time-scales of weeks to months with an amplitude in the V band of a few tenths of magnitudes. More spectacular are the variations in spectral type and $T_{\rm eff}$ on time-scales of years of up to about two magnitudes in V. These variations occur at roughly constant luminosity and are sometimes accompanied by changes in mass-loss rate.

LBVs are also famous for their outbursts: η Car showed a dramatic outburst in the 19th century when it ejected about 1 $M_\odot$ in a few decades (Andriesse et al. 1978; Hyland et al. 1979; van Genderen & Thé 1985). P Cyg had two outbursts in the 17th century (1600 and 1655) (see e.g. Lamers & de Groot 1992). In both cases, dust was formed in the ejecta. In the case of η Car direct evidence for circumstellar dust is found from infrared imaging and spectroscopy (Allen et al. 1985; Robinson et al. 1987; Smith et al. 1995; N. Smith et al. 1998). For P Cyg the direct evidence for cool dust is weak (Waters & Wesselius 1986), but the historic light curve strongly suggests obscuration due to dust formation (Lamers & de Groot 1992). Other luminous, but cooler massive stars, not classified as LBVs, can also show episodic dust formation due to enhanced mass loss, e.g. ρ Cas (G2Ia, e.g. de Jager & van Genderen 1989) and Var A in M33 ($T_{\rm eff} \sim 3$–8×10^3 K, Humphreys et al. 1987).

Almost all LBVs are surrounded by a dusty ring nebula (Nota et al. 1995). The underlying question we address in this

paper is: *what was the evolutionary state of the central star during the production of the dust shell observed today?* Two possibilities have been proposed in the literature: (i) dust production during LBV outbursts such as seen in P Cyg and η Car. The star may have been slightly cooler than at present during the outbursts; (ii) dust formed as a result of high mass loss during a (brief) period as a yellow or red supergiant (RSG). Another way to express these different scenarios is in terms of the envelope: did the star have a radiative or a convective envelope during the production of the dusty nebula? The latter case would correspond to an internal stellar structure of a RSG.

Observationally, it is plausible to assume that very massive stars, with main sequence masses above about 50 $M_\odot$, do *not* evolve into RSGs (Humphreys & Davidson 1979). The observed distribution of stars in the upper HR diagram shows a clear lack of RSGs above a luminosity of log ($L/L_\odot$) = 5.8, while there are many hot OB stars known with luminosities above that limit. This lack of RSGs is also observed for other galaxies (Humphreys & Davidson 1979). It is clear that either very massive stars never evolve to the RSG phase, or, if they do, this must be a very brief phase.

The dust in the nebula may be used in two ways to tackle the problem of their origin. First, by studying the composition of the dust. This may be different as a result of differences in the dust forming processes. Second, by studying the distribution and morphology of the dust in the nebulae, which may provide information about the mass-loss history during and/or after the dust formation process.

The LBV ring nebulae have a range of masses, between 10^{-4} and a few $M_\odot$ (Hutsemékers 1994). The chemical composition of these dusty nebulae shows evidence for CNO processing, which points to a stellar origin of the nebular material. Clearly, at some point in the recent past, the stars that are now LBVs have produced a dusty shell expanding at velocities of 20 to 60 $\mathrm{km\,s^{-1}}$ (a notable exception is η Car, whose ejecta move outward at a velocity of several 100 $\mathrm{km\,s^{-1}}$). The LBVs are believed to evolve into He-rich Wolf-Rayet stars, and evidence is presented that the ring nebulae observed in some of these stars are also the result of a phase of high mass loss via a dusty outflow (Smith 1997).

The nebular gas-phase abundances of LBV ring nebulae indicate enhancement of nitrogen (Smith 1997). Evolutionary calculations (Meynet et al. 1994), however, indicate that e.g. the surface N and He abundances are expected to be *higher* in the LBV stage than the abundances found in the nebulae of LBVs. This indicates that the envelope must have undergone some mixing, but that He-rich layers were not yet exposed to the surface of the star. Such a situation occurs in the RSG phase of massive stars. Indeed, L.J. Smith et al. (1998) propose that AG Car was a RSG when it ejected the dust shell.

In this paper we study the distribution and composition of the dust in two well-studied LBVs: AG Car and Wra 751. The latter star has been classified as a *candidate* LBV because it has not (yet) shown the characteristic variations in $T_{\rm eff}$ (Garcia-Lario et al. 1998) that AG Car shows. We use imaging of the dust shell to determine the location of the dust. This puts strong constraints on the grain size distribution when a model is used to fit the infrared thermal emission from the grains. We use infrared spectroscopy to determine the detailed shape of the dust spectrum and its solid state emission bands. These emission bands are telltale about the composition of the dust and hence provide valuable information about the physical and chemical conditions that prevailed during the dust formation process.

The paper is organised as follows: Sect. 2 gives an overview of the two objects studied in this paper. Sect. 3 describes the observations. In Sect. 4 we briefly describe the LWS spectra of the two objects. Sect. 5 contains a detailed description of the SEDs, using data obtained from many different telescopes. Ground-based infrared images are described in Sect. 6 and in Sect. 7 we use the data from Sect. 5 and 6 to construct model fits. In Sect. 8 we present an extensive discussion of the results and the last section contains a summary.

2. The stars

AG Car (HD 94910, IRAS 10541-6011) is one of the prototype LBVs, and one of the best studied examples of this class. It is a prototype LBV because:

1. It has a very high luminosity, log ($L/L_\odot$) $\simeq$ 6.2 (Lamers et al. 1989; Leitherer et al. 1994), assuming a distance of 6 kpc (Humphreys et al. 1989).
2. Its spectral type is known to change from early A to late O.
3. It shows large photometric and spectroscopic variations at optical and UV wavelengths (Spoon et al. 1994; Leitherer et al. 1994; Shore et al. 1996). V changed from 6.0 to 8.0 between 1981 and 1985 (Stahl 1986); stayed roughly constant until 1990 and reached 5.8 in 1994 (Spoon et al. 1994; Stahl 1997).
4. It has a circumstellar dusty ring nebula that contains CNO processed material (Thackeray 1950; McGregor et al. 1988; Nota et al. 1995; Lamers et al. 1996; Smith et al. 1997)

Thus AG Car fulfils all the primary LBV criteria: it is *Luminous*, *Blue* and highly *Variable*. It also fulfils a secondary criterion in that it is surrounded by a detached dusty nebula.

Wra 751 (Hen 3-591, IRAS 1065-6026) is a candidate LBV. It has the following characteristics:

1. It has a high luminosity, log ($L/L_\odot$) $\geq$ 5.7 (Hu et al. 1990), assuming a distance larger than 5 kpc. Van Genderen et al. (1992) determined the distance to be between 4 and 5 kpc. We adopt a distance of 4.5 kpc in this paper.
2. $T_{\rm eff}$ is not well determined but probably between 25,000 (Garcia-Lario et al. 1998) and 30,000 K (Hu et al. 1990)
3. It shows photometric variations of 0.15 mag on a timescale of months (van Genderen et al. 1992), but no significant variations in spectral type, typical for LBVs, have been observed.
4. It is surrounded by an almost circular dusty nebula (de Winter et al. 1992; Waters et al. 1997), which has a "significant" [N/O] overabundance of $3.0^{+3.0}_{-1.5}$ (Garcia-Lario et al. 1998).

Table 1. Log of TIMMI observations

Object	Date	Exp. time [min.]	Pixel size [arcsec]	λ_c [μm]	$\Delta\lambda$ [μm]
AG Car	25/2/94	59	0.66	12.56	1.41
	25/2/94	51	0.66	12.78	0.25
Wra 751	2/2/95	63	0.336	10.1	5.1

So, Wra 751 fulfils all LBV criteria except that up to now no large photometric and spectroscopic variations have been observed.

3. Observations

3.1. Ground-based imaging in the thermal infrared: TIMMI

Ground-based imaging around 10 μm was done with the Thermal Infrared MultiMode Instrument (TIMMI) (Käufl et al. 1994) at the 3.6m telescope at La Silla, Chile. A log of the observations is given in Table 1. The detector used was a 64×64 Ga:Si array, with a cut-off wavelength of 17.8 μm.

The maximum diameter of the optical nebula around AG Car is approximately 40 arcsec (e.g. Nota et al. 1995). Assuming the dust nebula to be of similar dimension, we chose the largest possible pixel size for TIMMI in order to be able to fit the entire nebula on the array. The optical nebula of Wra 751 subtends a smaller angle on the sky (diameter $\approx$ 22 arcsec, Hutsemékers & van Drom 1991, hereafter HvD), and it could be fitted on the array with a pixel size of 0.336 arcsec. In both cases the seeing was measured using a standard star and was approximately 1 arcsec. The Wra 751 image was flux calibrated, using α Cen as a flux standard, assuming a flux of 96 Jy in the N band. The images of AG Car have not been flux calibrated. The images were cleaned of high-frequency noise using a low pass filter. This technique is more effective in the case of high spatial sampling, so the Wra 751 image (where the point spread function (PSF) is about 3 pixels wide) benefited more than the AG Car images (PSF $\approx$ 1.5 pixel). In both cases we made sure that the full width at half maximum (FWHM) of a point source did not increase significantly as a result of the filtering technique. Further details concerning reductions of TIMMI images taken during the same run as Wra 751 are described by Voors et al. (1997).

3.2. ISO-SWS spectroscopy

Infrared spectroscopy of Wra 751 and AG Car between 2 and 45 μm was done using the Short Wavelength Spectrometer (SWS) (de Graauw et al. 1996) on board the Infrared Space Observatory (ISO) (Kessler et al. 1996). AG Car was observed on June 27th, 1996; Wra 751 on February 4th, 1996. For reduction of the data we made use of the SWS Interactive Analysis data reduction package (de Graauw et al. 1996). The Standard Processed Data (SPD), produced in pipeline processing version 5.0 or later, were dark subtracted, corrected for the relative spectral response function of the detectors, flux calibrated and corrected for spacecraft and earth's velocity. The SWS wavelength range (2.4 to 45 μm) is divided up into 4 different bands using 4 different detector blocks and two gratings. The maximum grating resolution $\lambda/\Delta\lambda$ is a function of the observed wavelength and lies roughly between 1,000 and 2,500. The AG Car spectrum was observed at $\sim$ 60 percent of the maximum resolution, the Wra 751 spectrum at $\sim$ 20 percent. Integration times were 6750 and 1256 second, respectively. No background measurements were performed. A more detailed description of the spectra and the way they were reduced is given by Voors (1999).

3.3. ISO-LWS spectroscopy

Spectroscopy in the wavelength range from 43 to 196 μm was done by using the Long Wavelength Spectrometer (LWS) (Clegg et al. 1996) on board ISO. AG Car was observed on February 4th, 1996 in LWS01 mode. Wra 751 was observed on September 10th 1996, also in LWS01 mode. For both stars a separate spectrum of the nearby background was obtained and subtracted from the on-source spectrum. The full wavelength range is sampled by moving the grating across ten different detectors simultaneously, five in first order (the long wavelength section: 84 to 196 μm), the other five in second order (short wavelength section: 43 to 93 μm). The spectra were oversampled by a factor of 4, which results in a resolution of 0.6 and 0.3 μm for first and second order, respectively.

Data reduction was done by T.L. Lim using the ISO Spectral Analysis Package (ISAP). First, glitches were removed by inspecting all ten detectors separately. In the case of the shortest wavelength detector, SW1, all scans (6) were inspected separately. Then, standard reduction procedures were performed (dark subtraction, response correction and flux calibration). Small differences in flux level between the different detectors (typically $<$ 10 percent) were corrected. The on-source spectra of each detector were scaled to fit the average spectrum since the differences between detectors are mainly due to a difference in gain. The background spectra of each detector were offsetted to fit the average spectrum, since at lower flux levels they are more due to differences in dark current between the detectors. The background spectrum was then subtracted from the on-source spectrum.

The final spectra have a resolution of $\lambda/\Delta\lambda \simeq 170$ and are shown in Figs. 1 and 2. A more detailed description of these spectra and the reduction procedures will be given by Barlow et al. (in preparation).

3.4. ISOPHOT-S spectroscopy

ISOPHOT-S spectra were obtained of AG Car on July 23rd 1996, and of Wra 751 on August 9th 1996, both with an integration time of 128 seconds, without chopping. Both wavelength ranges (2.5 to 5 μm and 6 to 12 μm) were observed. The spectral resolution of PHOT-S is about $\lambda/\Delta\lambda$ = 90. The effective size of the aperture of PHOT-S is 24 × 24 arcseconds. For a description of ISOPHOT we refer to Lemke et al. (1996).

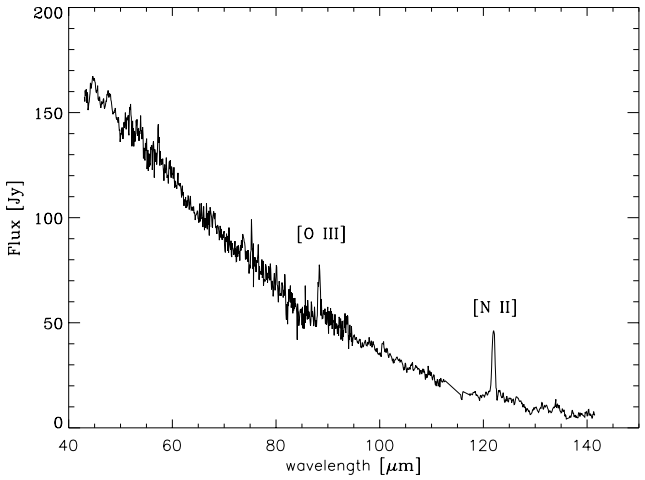

Fig. 1. Background subtracted LWS spectrum of Wra 751. Indicated are the lines of [O III] and [N II].

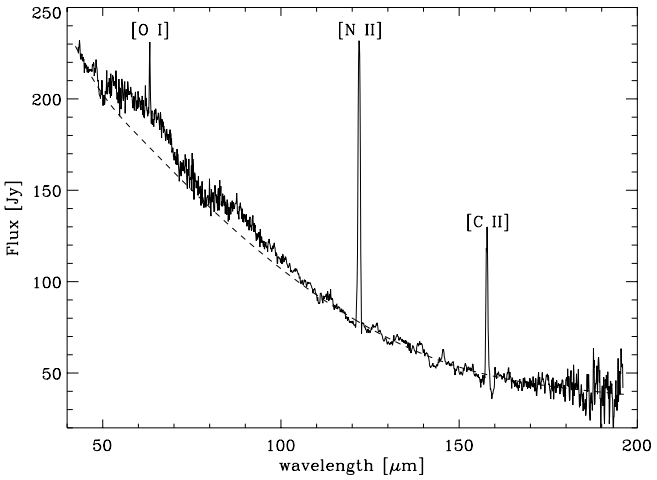

Fig. 2. Background subtracted LWS spectrum of AG Car. Indicated are the lines of [O I], [N II] and [C II]. The dotted line indicates the underlying continuum.

3.5. IRAS data

Infrared Astronomical Satellite (IRAS) data were obtained through the Groningen IRAS database. For Wra 751 the colour-corrected (Neugebauer et al. 1984) IRAS-point source catalogue (PSC) fluxes are used, except for the 100 μm point. This is listed as an upper limit in the PSC. From inspecting individual scans, we derived in a more accurate analysis a 100 μm flux of 25 $\pm$ 5 Jy. The large uncertainty in this flux is due to the high and complex background at this particular wavelength.

3.6. KAO data

The Kuiper Airborne Observatory data of AG Car, used in this paper, were taken from McGregor et al. (1988). Derived flux densities are 177 and 84 Jy at 50 and 100 μm, respectively. The uncertainty in the absolute flux calibration is $\sim$ 25 percent and there is a relative uncertainty of $\sim$15 percent. Scans taken across the nebula along the minor axis indicate that outside 30 arcsec from the stellar position no substantial dust emission at 50 and 100 μm is present.

3.7. SEST observations

AG Car was observed at 1.3 mm with the bolometer at the Swedish ESO Submillimeter Telescope (SEST) at La Silla, Chile on March 25, 1996, by P.A. Zaal. The planet Uranus was used as primary calibration source and was assumed to have a flux of 33.8 Jy at 1.3 mm. The derived flux of AG Car is 111 $\pm$ 20 mJy. Note that the beam of the SEST telescope at 1.3 mm is 20 arcsec, i.e. only the inner part of the nebula was observed.

4. The LWS spectra of Wra 751 and AG Car

The LWS spectrum of Wra 751 is shown in Fig. 1. Only one solid state feature appears to be present in the LWS spectrum of this star, located at 47.8 μm. This feature is also seen in AG Car, and may be interpreted as due to crystalline pyroxene. It is interesting to note that there are clear differences between the solid state structures seen in the LWS spectra of the two programme stars, whereas the spectra at shorter wavelengths (between 30 and 43 μm) are almost identical (Voors 1999).

Only two spectral lines are clearly visible: [O III]λ 88 μm and [N II]λ 122 μm. The [O I] λ 63 μm line does not appear to be present. This indicates that the ionized gas from where these lines originate, is hotter than in AG Car. In view of the effective temperature of the central star ($\sim$20,000 K, see Sect. 7.2) this is surprising. [O III] emission is usually not seen around stars with a B-type spectrum, but is more common in much hotter objects like Wolf-Rayet stars or planetary nebulae. We note that around the even cooler object G79.29+0.46 ($\sim$ 16,600 K, Trams et al. 1999) we detect [Ne III] emission, which is also not expected around such a cool source. It is speculated that shocks caused by the interaction with the surrounding medium may produce these high ionization lines. The spectrum longward of 140 μm is not shown because of a too low S/N ratio. Thus, the [N II] to [C II] ratio cannot be determined. Possibly there is also a [N III] line present at 57.3 μm, which would confirm the high ionization state of the gas surrounding Wra 751.

The LWS spectrum of AG Car is shown in Fig. 2. Indicated is an estimate for a smooth underlying continuum in order to enhance the visibility of weak features. The dust continuum is not entirely smooth; several structures are seen at the shorter wavelengths. There are narrow emission peaks at 48 μm. We interpreted this as due to crystalline pyroxene. Also, a broad structure around 60 μm appears to be present. Possible interpretations for this feature may also be pyroxene (Koike et al. 1993) or H_2O ice (Bertie et al. 1969). However, H_2O ice also produces a notable peak at 43 μm and the presence of such a feature in the SWS spectrum of AG Car is doubtful. There are also three strong spectral lines in the spectrum, [O I] λ 63 μm, [N II] λ 122 μm and [C II] λ 158 μm.

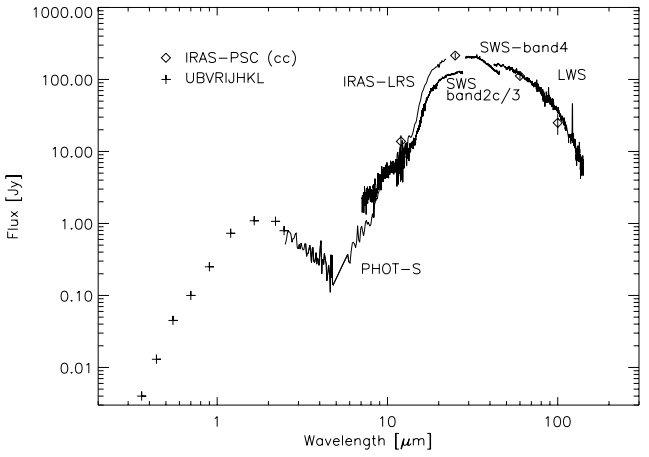

Fig. 3. Spectral energy distribution of Wra 751, combining data taken with different telescopes (see text). Optical and NIR photometry is from Hu et al. (1990).

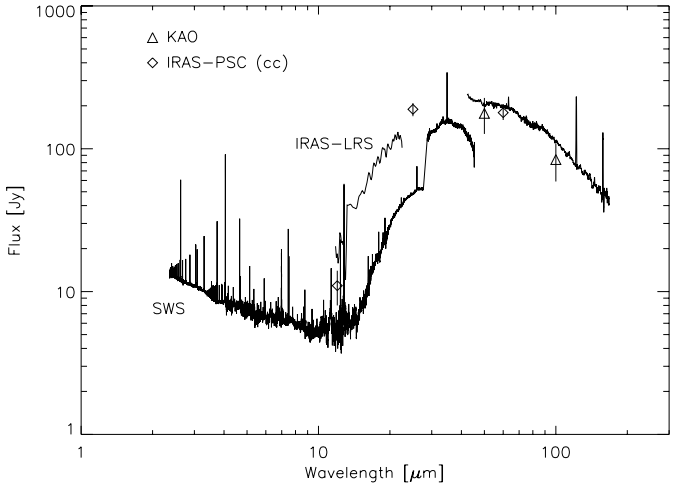

Fig. 4. Spectral energy distribution of AG Car, combining data taken with different telescopes (see text).

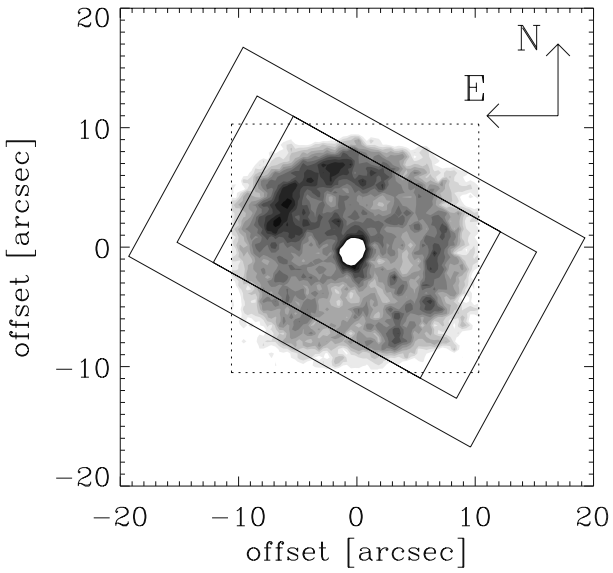

Fig. 5. N band image of Wra 751. North is up, east is to the left. The drawn lines indicate the orientation of SWS apertures (see text) during the observations. The dotted square box indicates the field-of-view of the N-band TIMMI image. The dashed circle indicates the limits of the low surface brightness Hα nebula (HvD).

5. Description of the spectral energy distributions

5.1. The spectral energy distribution of Wra 751

The spectral energy distribution (SED) of Wra 751 is shown in Fig. 3, and is characterised by two components: the star dominates shortward of 7 μm, and the dust shell longward of this wavelength. The optical and near-IR photometry was taken from Hu et al. (1990) and agrees well with the ISO fluxes. There is a significant difference in flux levels between the IRAS-LRS data and the ISO-SWS spectrum. This is due to the different apertures used in both spectrographs (note that the LRS was a slitless spectrograph) in combination with the spatial extent of the nebula (see Fig. 5). The flux level of the long wavelength point of the IRAS-LRS spectrum (23 μm) agrees well with the flux levels of the SWS band 4 spectrum near 30 μm. This implies that the large SWS band 4 aperture includes the bulk of the nebular emission at these wavelengths. At 45 μm, flux levels in the SWS and the LWS spectrum are in good agreement. LWS has a circular aperture of 80 arcsec diameter. We conclude that the IRAS LRS spectrum and the LWS spectrum represent emission from the entire nebula.

The solid state composition of the Wra 751 spectrum is discussed in detail by Voors (1999). We summarize their findings here. An amorphous silicate emission feature is found near 10 μm. In addition, weak narrow emission bands are seen near 33, 36, 40.5 and possibly near 43 μm. These features can be attributed to crystalline pyroxenes (Jäger et al. 1998).

5.2. The spectral energy distribution of AG Car

The SED of AG Car is shown in Fig. 4. The flux measurement at 1.3 mm is not shown. The optical photometry is not plotted because the star is highly variable in colour and magnitude. The SED of AG Car at short wavelengths ($2.3 < \lambda < 12$ μm) is dominated by the free-free emission from its wind. At longer wavelengths the SED is dominated by thermal radiation from the dust. The flux jump in the AG Car SWS spectrum at 29 μm is even more pronounced than in the case of Wra 751. This is not surprising given the larger angular size of the AG Car nebula (compared to the aperture of the SWS observations). There is even a flux jump between SWS band 4 and LWS at 45 μm. The flux levels of the LWS spectrum agree with the broad-band IRAS data at 60 and 100 μm (taken with a beam of 1.5×4.75 and 3×5 armin, resp.). This suggests that the entire infrared AG Car nebula fits within the LWS aperture. Also the KAO scans suggest that the dusty nebula is smaller than 60 arcsec across, i.e. well within the LWS aperture.

The solid state emission found in AG Car is remarkably similar to that of Wra 751: prominent emission near 33, 36, 40.5

and possibly near 43 μm is found, due to crystalline pyroxenes (Voors 1999). No evidence for a 10 μm amorphous silicate emission is found, probably due to the lower dust temperatures. Surprisingly, emission bands were found at 3.3, 7.7, 8.6, and 11.3 μm. These bands are usually attributed to Polycyclic Aromatic Hydrocarbons (PAHs) (Léger & Puget 1984) and suggest the presence of very small C-rich grains or large molecules in the AG Car dust shell. The formation of these small C-rich grains is not understood at present.

6. Description of the TIMMI images

6.1. The TIMMI image of Wra 751

The 10 μm broad-band image of Wra 751 (Fig. 5) shows an almost spherical distribution of emission, which is limb-brightened and peaks at a distance of about 7-8 arcsec from the central star. There is a marked asymmetry in the brightness distribution: the nebula is brightest in the north-east (NE), and it also shows some enhanced emission in the south-west (SW), but less pronounced. This asymmetrical distribution of surface brightness points to mass loss in a preferred direction (SW-NE). We note that HvD from Hα and [N II] imaging find that the eastern part of the nebula is brighter than the western part, roughly in agreement with our IR image. They also report a slight elongation of the nebula in the NW-SE direction, i.e. perpendicular to the density enhancement we observe in the infrared. Such a geometry is also seen in AG Car (see below). From long-slit spectroscopy (HvD), it is also apparent that the intensity of the [N II] line is stronger in the red-shifted part of the nebular emission than in the blue-shifted part. This would suggest that more material is receding from the observer than approaching. Note that the optical emission of the nebula is only seen in the lines and not in the continuum, i.e. it is not a reflection nebula (HvD).

The nearly circular appearance of the nebula, together with the centrally located star, suggest that any distortion of the brightness distribution in the nebula due to space motion of the central star is negligible. It also suggests that, while mass loss was enhanced in the SW-NE direction, the expansion velocity of the wind was about equal in all directions. Obviously, if a fast wind occurred after the ejection of the nebula, it did not (yet) strongly modify the geometry of the nebula. The modest present day mass-loss rate (10^{-6} M$_\odot$ yr^{-1}, Hu et al. 1990) and the low expansion velocity (190 km s^{-1}, HvD), are consistent with only modest wind-wind interaction.

A remarkable property of the nebula is its radial brightness distribution. We already noted the limb-brightening which is expected for a (spherical) detached envelope. However, the magnitude of the limb-brightening is less than expected for such a detached envelope and it is also different for the four quadrants of the nebula. To illustrate this point, we plot in Fig. 6 the average brightness as a function of radial distance from the star for the four quadrants, using annulae with a thickness of 1 arcsec (roughly the spatial resolution of the image). The contrast between the central part of the nebula and the brightest point at 7-8 arcsec is at most a factor 1.35 (Fig. 6). The observed ratio

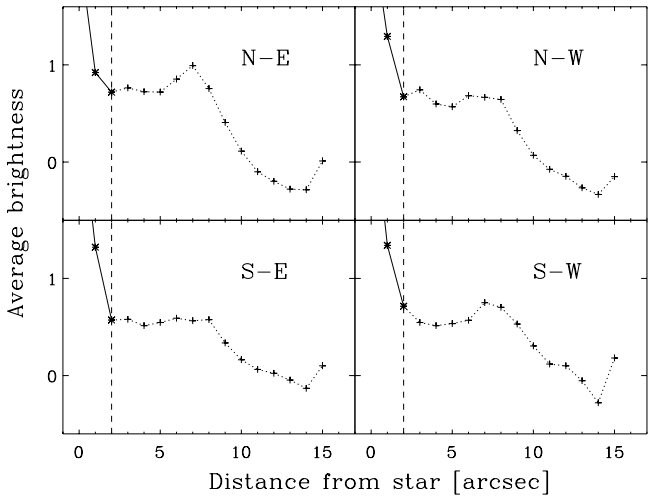

Fig. 6. Average surface brightness (in arbitrary units) of the four quadrants of the Wra 751 nebula as a function of radial distance from the star, as derived from the N-band image. The central star causes the sharp rise at the center of the image (0 arcsec). The vertical dashed line indicates the limits of the region still influenced by the stellar flux. Note the similar profiles for the NE, SW and for the NW, SE sections, and the weak or absent limb brightening.

of the limb-brightened edge to the central part of the nebula depends on (angular) thickness of the shell and on the resolution of the image. Using the parameters for the nebula of Wra 751 that we derive in Sect. 6.1, this ratio is approximately 3 when assuming infinite resolution, and 2.2 assuming the actual resolution of the image (1 arcsec). So, the N band image shows less limb brightening than expected for a spherical detached nebula, even in the NE-SW direction. The NW and SE quadrant do not appear to show any limb brightening at all.

Closer inspection of the optical image published by HvD shows that the central parts of the nebula, with a diameter less than 10 arcsec, are very bright, and that a fainter 'halo' extends up to a diameter of 22-23 arcsec. Our N-band image shows a peak in the brightness distribution corresponding to a shell with a diameter of 14-16 arcsec. The outer, fainter Hα halo corresponds to the peak in the IR brightness, and extends beyond it. Indeed, the large jump in flux observed in the SWS spectrum (see above) suggests that the cool dust extends well beyond the small 14x20 arcsec SWS band 3 aperture.

The long-slit spectra taken by HvD have been interpreted by them as due to a filled shell of emission rather than a detached shell. However, close inspection of the [N II] velocities measured by HvD shows a clear lack of line emission at zero velocity at most positions along the slit. Such line emission at zero velocity is expected in the case of a filled sphere of gas expanding at constant velocity. We conclude that the measured [N II] line shapes are *not* consistent with a filled spherical shell.

What then is the geometry of the gas and dust envelope around Wra 751? On the basis of the above discussed observations we suggest the morphology of the nebula to be as follows: the material is distributed in a torus, seen edge-on, of which the axis is oriented in the NW-SE direction (see Fig. 5). This ex-

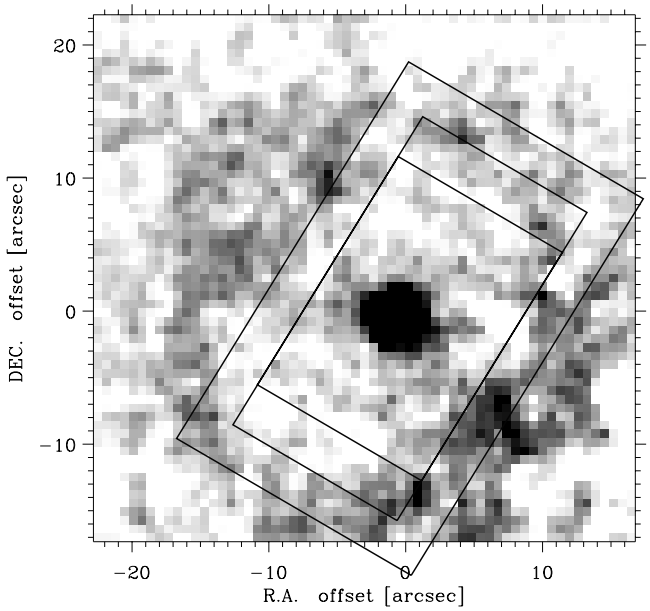

Fig. 7. AG Car and its surrounding nebula in the N3 band (λ_c = 12.5 μm). North is up, East is to the left. The boxes indicate the locations of the SWS apertures on the sky at the time of the SWS observation.

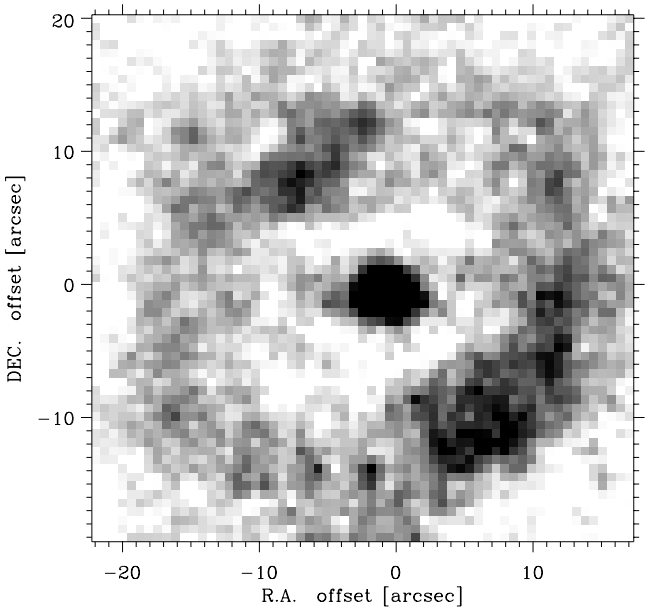

Fig. 8. Image of AG Car and its surrounding nebula taken through the [Ne II] filter (λ_c = 12.78 μm). North is up, East is to the left.

plains the relatively low surface brightness in these directions. The high surface brightness of the central part of the nebula suggests a non-homogeneous azimuthal distribution of material. As the [NII] line emission shows that there is more redshifted than blueshifted material, it is the back-side of the torus where the density of the material is highest.

Another notable feature of the 10 μm image is the brightness of the central source. The integrated flux of the unresolved central peak in the 10 μm image is 0.29 Jy; the total flux of star plus nebula is 5.87 Jy. As we will show in Sect. 5.1, the slope of the stellar spectrum between 2 and 5 μm suggests that at 10 μm the stellar flux is about 0.07 Jy. The measured flux of 0.2 Jy (i.e. 0.29 Jy minus the 'background' contribution) in the TIMMI image therefore indicates the possible presence of an extra contribution very close to the central star. It is likely that this is another dusty component very close to the star. The long-slit spectrum of HvD also shows the presence of an unresolved nebular contribution. Contrary to the extended nebula, the blueshifted and the redshifted peak of this unresolved component are of equal strength. A spatially unresolved spherical shell at constant velocity is expected to produce a flat-topped line profile and not a double-peaked profile. This suggests that this unresolved component is either not spherically symmetric or rotating.

6.2. The TIMMI images of AG Car

The 12.5 μm N3 band image of AG Car shows a slightly elongated ring roughly in the NW-SE direction around a bright central star (cf. Fig. 7). The SW section is the brightest part of the nebula, and also the NE is brighter than the NW-SE axis. The maximum brightness at the SW and NE of the star is located approximately 11 arcsec from the star. This coincides perfectly with optical continuum band images, which show the reflected stellar light on the dust particles (Nota et al. 1995). However, we note the presence of a second component in the NE direction at a distance of about 18 arcsec from the central star, not seen in optical continuum band images.

The [Ne II] λ 12.78 μm image (Fig. 8) shows a similar morphology to the N3 band image: an elongated ring in the NW-SE direction which is brightest perpendicular to this axis. The SW is the brightest section of the ring. This image too, coincides perfectly with the Hα + [N II] images shown by Nota et al. (1995). The [Ne II] image appears to be smoother than the N3 image of AG Car, however the S/N is limited. Optical images clearly show that the gas is distributed more smoothly than the dust (Nota et al. 1992).

We note that as a result of the large width of the N3 band ($\Delta\lambda$ = 1.41 μm), it also includes the [Ne II] line. However, the total line flux of the [Ne II] line in the SWS spectrum is only 12 percent of that of the continuum between 11.9 and 13.3 μm. If we also take into account the wavelength dependent transmission of the N3 band, which peaks at 12.56 μm, the relative contribution of the [Ne II] line is even smaller. So, if we assume that the [Ne II] line over continuum ratio is constant throughout the nebula, the [Ne II] line contributes only on the order of 10 percent of the total flux in the N3 band. Vice versa, the [Ne II] image is 'contaminated' by the continuum. The continuum accounts for roughly half of the flux. So we conclude that the N3 image indeed shows the continuum emission, whereas the [Ne II] image also shows a significant contribution from the continuum.

The ring-like structure suggests that the AG Car nebula is in a detached shell, with an increased amount of matter in the NE-

SW direction. This is true for both the [Ne II] image and the N3 band image. These images spatially coincide, indicating that the gas and the dust are co-spatial (i.e. within the resolution of the TIMMI images). Higher resolution HST optical images (Nota et al. 1995) show a very clumpy V-band nebula, indicating that the dust in the AG Car nebula may be in self-shielding pockets. Recent observations by Marston et al. (1999) show that CO is present as well in the nebula, and moves outward with a velocity of 30 km s^{-1}. This is much lower than the average outflow velocity of the gaseous nebula (70 km s^{-1}, Smith 1991).

7. Model fits to IR spectroscopy and imaging

In this section we describe the results of applying a radiative transfer code to model a number of SWS spectra in order to derive some properties of the circumstellar dust. A description of the SWS-spectra of Wra 751 and AG Car are given elsewhere (Voors 1999). Our modelling has several advantages over previous efforts (Smith 1991; Nota et al. 1992; Hutsemékers 1994). First, previous dust model fits were made by using only a few photometric points. Here we use the entire spectrum from 2-200 μm. Second, having a *spectrum* also allows to determine the composition of the dust much more accurately than previously possible. Third, we use ground-based infrared imaging, to determine the spatial extent of the dust. Also, the ISO-SWS and LWS apertures put strong constraints on the angular size of the nebulae.

Since similar data for both objects were available, and since the objects are very similar in appearance, the same method to fit the images and the spectra of the two objects was applied. The basic steps are the following. First, the stellar parameters are determined. Given the distance to the object, the observed *angular* size of the nebula (from the images) determines the *physical* size of the nebula; the inner radius is determined by the peak in the brightness level, the outer radius is much less well determined. The spectra constrain the dust composition, while the assumption of thermal equilibrium of the dust grains in combination with information about the spatial distribution of the dust constrain the dust size distribution. The physical size, combined with the density distribution, then gives the total dust mass of the nebula. The details of the model fitting procedure are explained for each object separately.

7.1. Dust modelling program: MODUST

We have used a 1-D radiative transfer code to model the dust emission from the dust shells of Wra 751 and AG Car. The program, MODUST, will be described in more detail elsewhere (de Koter et al., in preparation). Here we give a brief overview. The program models the emergent spectrum of a spherical dust shell around a central star. A library of Kurucz (1991) models is available, though any given spectrum may serve as input spectrum. The model assumes the grains to be in thermal equilibrium with the radiation from the central star. Optical depth effects are taken into account. The model dust shells that are discussed in this paper are all optically thin ($\Delta\tau_{\rm shell} < 0.2 \; \forall \; \lambda$). Tables of optical constants for each dust component are required as input for the program. A library containing these data for some fifty dust types from different dust families and lattice states is available. Any given power-law grain size distribution can be used and various dust shapes can be adopted (spherical, elliptical etc.). In case of spherical grains, a Mie code is used to calculate the emissivity of the dust. In the case of non-spherical grains, we use a continuous distribution of ellipsoids (CDE). However, due to computational limitations CDE can only be used in the Rayleigh limit of small grains ($\lambda \gg 2\pi a$, where a is the grain size). The emergent spectrum can be computed in two ways. First, the total flux of the dust shell is calculated, and second, the flux through the different SWS and LWS apertures is calculated, which allows us to model the flux jumps due to changes in aperture size at the boundaries of the SWS spectral bands.

7.2. Wra 751

The angular size of the nebula around Wra 751 almost exactly matches that of the largest SWS aperture. This means that at longer wavelengths ($\lambda > 29$ μm) nearly the entire nebula fits within the SWS aperture, whereas at shorter wavelengths flux will be lost. The predicted emergent spectrum and 2-D image on the sky are subject to the constraint of the observed 10 μm image of the nebula (Fig. 5).

Since both the luminosity and the effective temperature of the star are uncertain, we decided to fit the spectrum and the image using a range of input values for the stellar parameters. The most often quoted literature value of the luminosity is 5×10^5 L$_\odot$ (e.g. Hu et al. 1990), but we also tried models for luminosities of 3×10^5 and 8×10^5 L$_\odot$, which are typical values for LBVs. The values for the temperature in the literature are all between 20 and 30 kK, so we tried stellar input models of 20, 25 and 30 kK.

From the TIMMI image we know that the inner radius of the dust shell is located at approximately 8 arcsec from the star. At a distance of 4.5 kpc this corresponds to 0.17 pc. The outer radius is less well confined, since no millimeter observations of Wra 751 are available. A mild constraint is given by the uncertain 100 μm IRAS flux of 25 Jy and by the shape of the LWS spectrum.

From the observed spectrum it is clear that silicates are present, as indicated by the 10 μm emission bump. At longer wavelengths we also observe some structure that indicates the presence of crystalline pyroxenes (Voors 1999). Unfortunately, at present there are no reliable optical constants available for crystalline Mg-rich pyroxenes. The identification of the solid state bands given by Voors (1999) is based on transmission data of synthetic enstatite (Koike et al. 1993), whose optical constants still await determination. More recent laboratory data on pyroxenes (Jäger et al. 1998) do not reproduce the observed band strengths very well. This is probably due to minor chemical impurities and/or a non-negligible Fe content. Since the amount of crystalline dust is small, we decided not to include this component in our model fits. So the main ingredient with which we

model the spectrum is some form of amorphous silicate. Many different types of both amorphous olivines and pyroxenes were used to attempt a best fit. Olivines tend to produce a too high flux around 30 μm, pyroxenes give a better fit. From our data it is difficult to determine the fraction of Fe included in the amorphous dust, but a 50/50 Fe to Mg abundance yields good results. We therefore used this material to fit the overall shape of the dust shell.

Our best fit model is shown in Fig. 9. The stellar parameters are $T_{\rm eff}$ = 20,000 K and R = 50 $R_\odot$, implying log ($L/L_\odot$) = 5.56. A Kurucz (1991) model with the above parameters was used as an input spectrum. The mass-loss rate of the central star is low ($\dot{M} \approx 10^{-6}$ $M_\odot$ yr^{-1}; Hu et al. 1990), so free-free radiation does not play an important role in the determination of the stellar continuum flux between 2 and 12 μm. The stellar parameters are derived from optical and NIR photometry, assuming $E(B-V) = 1.7$ (Hu et al. 1990: 1.8; Garcia-Lario et al. 1998: 1.5). The inner radius of the dust shell is 1.5×10^5 $R_\star$, the outer radius is twice as large, 3.0×10^5 $R_\star$. A Mathis-Rumple-Nordsieck (MRN, 1977) size distribution of the dust particles was assumed ($n(a) \propto a^{-3.5}$), with cut-off wavelengths of 0.03 and 1 μm. The density distribution of the dust shell was assumed to be $\propto r^{-2}$. The total dust mass of the shell is 1.7×10^{-2} $M_\odot$. A shell with a constant density was also tried, and this gave a satisfactory fit as well. Such a density profile is often assumed for evolved planetary nebulae. The mass of this shell only increased by 10 percent with respect to the r^{-2} case. So, based on our modeling we cannot conclude what the density distribution is of the dust shell surrounding Wra 751. The reason that both density distributions give equally good fits, with similar masses, is that almost the entire emission from the dust shell is dominated by conditions at the inner radius. The outer radius contributes mostly at longer wavelengths, but because the shell is relatively thin, the temperature difference between the inner and outer radius is small. For the smallest particles the temperature at the inner radius is 102 K, at the outer radius 82 K.

The model gives a good fit to the overall shape of the spectrum. As expected, there are different flux losses through the different SWS apertures. The amount of flux lost is well predicted in our model. However, there are two regions where the model deviates significantly from the observations. First, in the model there is a peak around 20 μm. This peak is the result of assuming spherical particles in the calculation of the optical properties of the dust particles. If we assume a continuous distribution of ellipsoids (CDE) for the particle shapes, this peak around 20 μm disappears. However, the grain sizes in the applied CDE code can only be treated in the Rayleigh limit, which is not applicable to our adopted grain sizes. Therefore we use the MIE code to determine the overall shape of the energy distribution and CDE to investigate the effect of changing the grain shape distribution.

The second discrepancy occurs between 5 and 15 μm. Both the PHOT-S and the SWS spectra show a higher flux than the model. This indicates that a population of warm grains has to be present around Wra 751. The 10 μm TIMMI image shows that these grains are mainly in the detached shell or in the thin, high

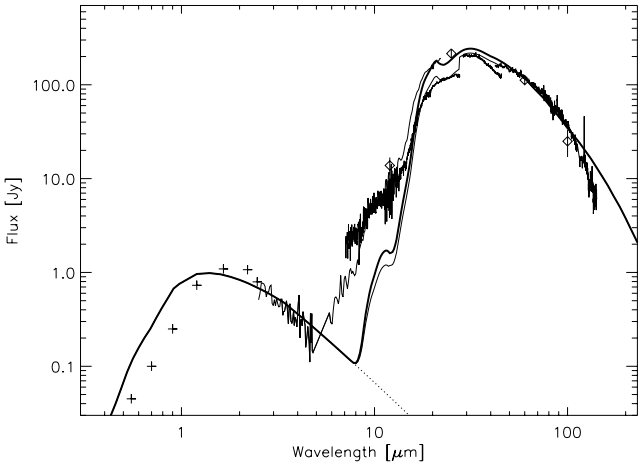

Fig. 9. Dust fit to the ISO spectrum of Wra 751. Symbols have the same meaning as in Fig. 1. The thick line is the (reddened, E(B-V) = 1.7) model without apertures, the thin line is the model taking the SWS-apertures into account, the dotted line indicates the stellar contribution.

surface brightness layer also seen in Hα and [N II]. Therefore, these grains cannot be in thermal equilibrium and must be much smaller than the bulk of the grain population. If we add a very small amount ($\approx$ 1 percent of the silicate dust mass) of very small carbon grains (10^{-2} μm) to the silicate grains, the lack of emission is perfectly filled up. The temperature of these grains is roughly150 K, so much warmer than the larger silicate grains.

The difference between the model and the LWS spectrum beyond $\sim$ 100 μm may very well be due to a very uncertain absolute flux calibration because of the low flux levels (less than 10 Jy). Therefore in determining the best fit, we have given this region a low weight.

We point out that the optical long-slit [N II] spectra (HvD) indicate the presence of a spatially unresolved, non-spherical shell of gas close to the star expanding at velocities comparable to those of the detached shell. Hence, this [N II] emission is not from the present-day wind which expands at much higher velocities. The flux at 10 μm of the central point source in the TIMMI image suggests a significant excess flux over that expected for the star, which we interpret as due to thermal emission from dust grains. Thus, the optical and TIMMI data both suggest that Wra 751 recently had another brief dusty mass-loss episode, and that this mass loss was non-spherical.

The expansion velocity of the detached gaseous nebula is 26 km s^{-1} (HvD). This means that with inner and outer radii of the dust shell of 1.5×10^5 and 3×10^5 $R_\star$, respectively, and a total dust mass of 1.7×10^{-2} $M_\odot$ the average dust mass-loss rate when the shell was formed was 2.7×10^{-6} $M_\odot$ yr^{-1}. Assuming a gas/dust ratio of 100, this gives a total mass-loss rate in the order of 2.7×10^{-4} $M_\odot$ yr^{-1} for a period of 6300 yrs. The assumed gas/dust ratio is the canonical value for the Galactic interstellar medium. It is difficult to establish the error we make by assuming the same value for the circumstellar environment of Wra 751. The total duration of the shell episode depends critically on the assumed outer radius of the shell, which is uncertain by at least a factor of two.

The derived total dust mass is also influenced by the uncertainties in the optical constants. One source of uncertainty is that the materials used in the laboratory are not the same as those found around the stars. Another source of uncertainty is the Fe-content. The more Fe the grains contain, the stronger the absorption at short wavelengths and the stronger the resonance. Thus, if the real Fe content is higher than the assumed 50 percent, the total mass will be less. However, a higher Fe content also causes the grains to be hotter at the same distance from the star. Since we know from the images where the dust is located, we can constrain the Fe content reasonably well and we estimate the error to be on the order of 10 percent. Thus, we expect that the uncertainty in the derived total mass as a result of the uncertainties in the dust properties is on the order of tens of percent. This is much less than the error caused by the uncertainties in the nebular parameters (see above), so we estimate a total uncertainty in the total mass to be at least a factor of two.

7.3. AG Car

Model fitting of AG Car was done in much the same way as Wra 751. First, the SWS spectrum of the central star – up to $\sim$ 12 μm – was fitted with a spherical non-LTE model atmosphere, which treats the stellar photosphere and the present-day stellar wind in a unified manner (de Koter et al. 1993, 1997). So, no artificial separation between star and wind as is done in the core-halo approach is made. We adopted $T_{\rm eff}$ = 20,000 K and $R_\star$ = 139 $R_\odot$, which gives log(L/L$_\odot$) = 6.44. This value agrees with the value of 6.22 ± 0.2 given by Lamers et al. (1989). In order to match the slope of the continuum in the NIR, we needed to adopt the following wind parameters: $\dot{M} = 1.4 \times 10^{-4}$ M$_\odot$ yr^{-1}, $v_\infty = 150$ km s^{-1}. The velocity law is assumed to be a β-type, with β equal to unity. These parameters are consistent with those derived by Leitherer et al. (1994) from detailed model fitting using similar unified models. A correction for interstellar extinction of $E(B-V) = 0.63$ (Humphreys et al. 1989) was applied. The stellar model predicts a V-band magnitude of 6.52 (assuming a Savage & Mathis 1979 extinction law) which agrees reasonably well with the 6.7 mag as observed by the RASNZ a few days before and after the SWS observations were done (Mattei 1999, priv. comm.).

Given the similarity of the continuum subtracted solid state spectra (Voors 1999) of Wra 751 and AG Car, we assume the same dust composition. For Wra 751 it was shown that it is likely that pyroxenes, both amorphous and crystalline, constitute the major contribution to the total dust content. Contrary to Wra 751, however, AG Car also shows emission from the well-known emission bands at 3.3, 7.7, 8.6, 11.3 and possibly also at 6.2 μm, usually attributed to Polycyclic Aromatic Hydrocarbons (PAHs). The presence of these features in the spectrum shows that very large molecules/very small dust particles are also present around AG Car. We will return to the implication of this observation below.

The infrared images of AG Car show that most of the emission comes from the NE-SW axis. These regions are approximately 11 arcsec away from the central star. The NW-SE axis is approximately 16 arcsec away from the central star. Assuming spherical symmetry obviously introduces uncertainties in the fit, but it is clear that the angular size of the nebula in the model should be around 12 to 13 arcsec. We assumed an angular distance of 12.5 arcsec, which at a distance of 6 kpc translates to a radius of 0.36 pc.

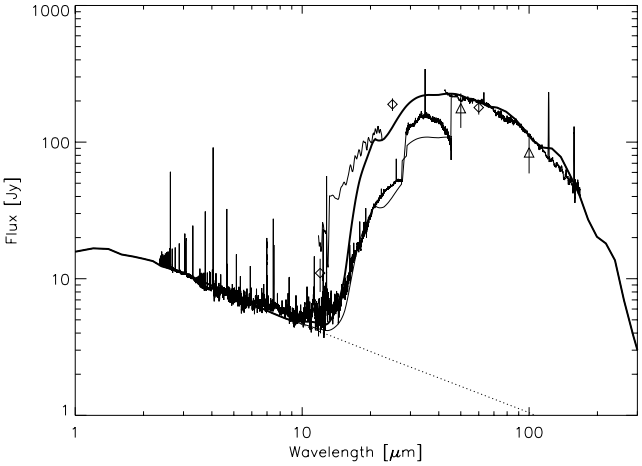

Fig. 10. Dust fit to the ISO spectrum of AG Car. Symbols have the same meaning as in Fig. 2. The thick line is the (reddened, E(B-V) = 0.63) model without apertures, the thin line is the same model taking the SWS-apertures into account, the dotted line indicates the stellar contribution.

Given the photometric and spectroscopic variability of AG Car, it is not immediately clear what temperature of the central star should be used as input spectrum. The temperature of 20,000 K mentioned above is only some average value. We therefore investigated the influence of a change in effective temperature on the dust emitting properties of the dust shell, keeping the luminosity fixed. AG Car is known to remain at constant luminosity during its variations (Lamers et al. 1989). Kurucz (1991) models with temperatures of 15, 20, 25 and 30 kK were tried, and they did not result in significant change in the emergent spectrum of the dust shell. Larger differences are expected if $T_{\rm eff}$ drops below 10,000 K, but such a low value has not been observed so far for AG Car.

Our best fit model is shown in Fig. 10. The inner and outer radii of the dust shell are 1.2×10^5 and 2.6×10^5 $R_\star$. The total dust mass is 0.25 M$_\odot$. We assumed an MRN grain size distribution, and derived cut-off sizes of 0.25 and 40 μm. The size of the smallest particles is determined by the inner radius of the dust shell, that of the largest particles is determined by the assumed outer radius and the slope of the LWS spectrum. We assumed a density gradient proportional to r^{-2}. We also tried to fit the model with a flat density gradient (ρ constant). This also led to a good fit, with the same inner and outer radii and a very similar mass (only 10 percent larger than the r^{-2} case). The reason that both density distributions give equally good fits, with similar masses, is that the temperature difference between the inner and outer radius is small (see also Wra 751). For the smallest particles the temperature at the inner radius is 99 K, at the outer radius 76 K.

Based on our model fit we note that the high mm-flux of 111 $\pm$ 20 mJy results from free-free emission in the dense, ionized present-day stellar wind (not shown in Fig. 4). The model calculations for the unified model atmosphere are consistent with the observed flux. It should be noted that the millimeter observations and the ISO-SWS observations were not done at the same time, but 3 months apart. Our model does not predict a high mm-flux from the dust shell. However, the beam size of the SEST is 20 arcsec, so a considerable amount of the cold dust may in fact be outside this aperture. We note that there is apparently no large contribution from non-thermal emission to the millimeter continuum in the present-day stellar wind.

As in the case of Wra 751, our model also gives a satisfactory fit to the size of the jump in flux levels at 29 and 45 μm. In Fig. 10, we show both the overall fit of the spectrum as well as the ISO-SWS aperture corrected spectrum. We see that the ISO-SWS spectrum is reproduced well. The first difference we note is the peak in the model spectrum around 20 μm which is completely absent in the ISO-SWS spectrum. The explanation for the predicted presence of this peak is identical to a similar occurence in Wra 751 (see Sect. 7.2). It results from the assumption of spherical particles.

From Fig. 10 it is clear that our model fails to explain the flux between $\sim$14 and 20 μm; there is a significant difference between the model and the IRAS-LRS flux levels. The PHOT-S spectrum (not shown) was taken less than a month after the SWS spectrum and its flux levels are fully consistent with it. In view of the differences in aperture size at these wavelengths (PHOT-S: 24 $\times$ 24 arcseconds and SWS:14 $\times$ 20 arcseconds), this shows that this emission likely is entirely due to the central star and not to some extended source. As in the case of Wra 751 (see above) and R 71 (Voors et al. 1999), there seems to be a small excess of warmer grains. We do not see this excess in the aperture-SWS spectrum. There the model fluxes agree reasonably well with the observed spectrum. Thus, we conclude that even though these are apparently hot grains, they seem to be located predominantly outside the SWS-aperture shortward of 20 μm, i.e. the grains are in the detached nebula. The presence of PAH emission is another indication for the presence of small grains. As in the case of Wra 751 we need only a very small amount (in this case only 0.1 percent of the silicate mass) of very small (10^{-2} μm) grains in order to fill up the deficit. The temperature of these grains is on the order of 180 K.

The average expansion velocity of the AG Car nebula is 70 km s^{-1} (Smith 1991; Nota et al. 1992), though higher velocity material also seems to be present in the ejecta (Thackeray 1977). With the above nebular parameters, this gives a dust mass-loss rate of 3×10^{-5} M$_\odot$ yr^{-1} over a period of 6000 years. This phase ended approximately 6×10^3 years ago. If we assume a canonical value of 100 for the gas/dust ratio, AG Car had a total mass-loss rate of 3×10^{-3} M$_\odot$ yr^{-1}. It should be noted that both the dust mass and the assumed gas/dust ratio are uncertain by probably a factor of 2.

Compared with previous determinations of the nebular parameters, the main difference is in the total dust mass of the shell and hence its time-averaged mass-loss rate. Previous determinations of the age of the nebula and the predominant grain temperature agree well (Hutsemékers 1994; Nota et al. 1992; McGregor et al. 1988). However, because of a lack of reliable data longward of 60 μm, the total dust mass has thus far always been underestimated by almost an order of magnitude.

8. Discussion

In this section, we discuss several aspects of the dust nebulae of Wra 751 and AG Car, and we speculate about the formation history of the nebulae. In Table 2 we list similarities and differences between the two objects.

8.1. dust composition and nebular mass

The dust mass contained in both nebulae (0.02 M$_\odot$ for Wra 751 and 0.25 M$_\odot$ for AG Car) is substantial, but entirely consistent with a stellar origin. A stellar origin is also inferred from the enhanced N abundance in the ionized part of the nebulae (HvD; L.J. Smith et al. 1998). We stress that the derived dust masses depend on the maximum grain size adopted and uncertainties in the optical constants, and are uncertain by a factor 2. Previous dust mass estimates (McGregor et al. 1988; Nota et al. 1992; Hutsemékers 1997) suffer from larger uncertainties because of the unknown dust composition, less accurate optical constants, and less well constrained (geometrical) nebular parameters.

We can compare the nebular dust- to gasmass determinations based on either optical or CO line observations. For Wra 751, HvD quote an uncertain gas mass of 3.2 M$_\odot$ based on Hα. Clearly, this only reflects the ionized mass in the nebula, and our analysis indicates that the bulk of the dust is outside the ionized region. Unfortunately, no measurement of the neutral component of the gas in the nebula is available. An upper limit to the total mass in the Wra 751 shell can be found by assuming that the ionized gas and dust are not mixed. In that case, adopting a gas/dust ratio of 100 for the neutral envelope, we find an upper limit to the total mass of 5.2 M$_\odot$.

For AG Car, an ionized gas mass of 4.2 M$_\odot$ was found by Nota et al. (1992) based on Hα. Marston et al. (1999) find a neutral gas mass of about 3.6 M$_\odot$ based on CO rotational line emission, while a dust mass estimate of 0.25 M$_\odot$ is derived in the present study. The optical and IR images of the AG Car nebula indicate that the ionized gas and the dust are co-spatial. For a gas to dust ratio of 100, we derive a nebular mass of 25 M$_\odot$ based on the dust. The sum of neutral (CO) and ionized (Hα) gas mass is 8 M$_\odot$. The discrepancy between these two numbers may indicate that the gas to dust ratio is only $\sim$ 32.

The grain size distribution required to fit the ISO spectra and the ground-based images points to (on average) large grains. For AG Car even very large (up to 40 μm) grains are needed in order to reproduce the high flux levels seen in the LWS spectrum. Smaller grains would require a more extended dust shell which is not in agreement with the KAO data and the observed flux jumps in the ISO spectrum.

Alternatively, the grains in AG Car could have different scattering and absorption efficiencies than those used in the model

Table 2. Overview of similarities and differences between the nebulae around Wra 751 and AG Car discussed in this paper.

Similarities	Differences
• Roughly spherical distribution of emission; marked asymmetry in brightness pointing to mass loss in preferred direction. Slight elongation of nebula in direction perpendicular to the density enhancement – suggesting roughly constant expansion velocity in all directions	• Optical emission in Wra 751 only seen in lines, not in continuum. In AG Car nebula seen in both.
	• Optical (Hα) image of Wra 751 different from infrared image; Hα nebula probably scattering nebula containing cold dust particles. Optical AG Car images coincide with infrared images.
• Both dust shells detached.	• AG Car nebula more elongated than Wra 751.
• Both stars show presence of a population of (small non-TE) warm grains. These are also seen around other LBVs and Wolf-Rayet stars.	• AG Car shows presence of PAHs, Wra 751 does not.
	• Wra 751 shows amorphous silicates (at 10 μm), though not very pronounced. AG Car lacks amorphous silicate emission, suggesting warm grains are not composed of amorphous silicates
	• Wra 751 has neutral gas outside dust region and ionized gas is only present in inner part of the dust region; in AG Car ionized gas only and gas and dust are co-spatial. Difference may be explained if Wra 751 is less evolved.
• Similar continuum subtracted solid state spectra, in which pyroxenes constitute major contribution to total dust content.	
• Little or no crystalline olivines are found. This seems to follow a trend towards higher pyroxene over olivine abundance in RSGs compared to lower luminosity AGB stars.	
• Both stars show on average large grains, in agreement with sizes found in RSGs and larger than grains of lower luminosity AGB stars.	• AG Car shows very large grains.
	• Wra 751 recently showed another brief dusty mass-loss episode in a non-spherical wind, indicated by the [N II] emission close to the star.

calculations. For instance, a higher albedo in the optical and ultra-violet would lead to less efficient absorption and thus lower grain temperatures. We would then overestimate the grain size required to fit the spectra and images. It is possible to increase the albedo of refractory materials (such as silicates) using an icy mantle, e.g. crystalline H_2O ice. This would result in prominent solid state emission bands at 43 and 60 μm. Indeed, emission at these wavelengths is observed in AG Car, but at modest strength. It is not fully clear whether these emission bands can be attributed to crystalline H_2O ice, since crystalline pyroxenes also produce emission near these wavelengths (Koike et al. 1993). This issue remains open at present, but introduces some uncertainty in the derived sizes of the largest particles. Since we cannot include such core-mantle particles in our model calculations, it is difficult to determine how large the influence will be on the derived particle sizes and hence on the dust mass.

If a significant fraction of the dust grains around AG Car are indeed larger than 10 μm, we should consider their formation history. As noted below, the maximum grain size observed in *outflows* is of the order of a micron, whereas much larger grains are only found in long-lived *disks*. Let us first assume the possibility of grain growth in an outflow. Once the gas from which the dust particles form contains enough seeds, grains will grow on these critical clusters. In general one could say that the lower the critical cluster density, the less they have to "compete" for available atoms or molecules, such that larger grains can grow. So, if for some reason the cluster density in the outflow of AG Car was very low, this may have resulted in very large grains. However, as noted above, very large grains are predominantly found in long-lived disks and *not* in outflows. One could propose that the dust particles in the present-day nebula, have been in a circumstellar disk for a sufficiently long time. One indication that a disk could be or could have been present in the AG Car system is the elongated shape of the nebula. It is not clear, however, how long the pristine dust particles have to be in a disk for substantial coagulation to take place.

In the case of AG Car it was noted before that the nebula contains predominantly large grains (> 1 μm, McGregor et al. 1988). The wavelength independent ratio of the nebular and stellar IUE spectra (Viotti et al. 1988) up to 3000 Å also suggests that the scattering particles are much larger than 0.05 μm in size. Jura (1996) finds that typical grain sizes for some massive RSG are larger than for lower luminosity AGB stars. Seab & Snow (1989) require large grains (> 0.08 μm) to fit the circumstellar UV extinction of the RSG α Sco, and Rogers et al. (1983) find grain sizes of 0.1 or 0.5 μm for the RSG μ Cep. These observations suggest that RSG have larger grains than lower luminosity AGB stars.

Both nebulae studied in this paper contain crystalline pyroxenes and little to no crystalline olivines (Voors 1999). From ISO-SWS spectroscopy of a larger sample of AGB stars and RSGs, Molster et al. (in preparation) show that there is a trend towards a higher abundance of pyroxenes for RSGs compared to lower luminosity AGB stars. AG Car and Wra 751 seem to follow this trend, to the extent that they show only crystalline pyroxenes and no strong evidence for crystalline olivines. We conclude that both the grain size distribution as well as the dust composition point to conditions in the dust formation regions of AG Car and Wra 751 that may have been similar to those observed in RSG.

In both nebulae a minor population of very small grains is found that is not in thermal equilibrium with the stellar radiation field. Not much mass is contained in these grains, but because of their high temperature they radiate effectively and therefore they are easily detectable at the short-wavelength part of the dust spectral energy distribution. These small grains only produce continuum radiation in Wra 751, and continuum and emission in the PAH bands in AG Car. The lack of prominent silicate emission from these warm grains suggests that they are not composed of silicates. The case of AG Car proves that at least some grains (the PAHs) are in fact C-rich large molecules or very small grains.

AG Car and Wra 751 are not the only massive stars with dust shells containing small grains not in thermal equilibrium. In the LBV R71 in the LMC, Voors et al. (1999) discovered the presence of PAH emission and a prominent warm grain component which could not be fitted using thermal equilibrium grains in the detached dust shell. Also, emission from PAH molecules in HD 168625 indicates the presence of non-equilibrium grains in this lower luminosity LBV (Skinner 1997). From a study of dust in WR ring nebulae consisting of stellar ejecta, Mathis et al. (1992) found a prominent population of very small grains in addition to more usual grain sizes. There may be an evolutionary link between the WR ring nebulae and LBV ring nebulae, since it is believed that LBVs evolve into WR stars. Our results concerning the grain populations in AG Car and Wra 751 support such an evolutionary relation between LBV and WR ring nebulae.

At present the origin of the small grains in LBV ring nebulae and in WR ring nebulae is still unclear. It is possible that larger grains are destroyed by the effects of the fast wind of the central star on the slowly expanding, dusty ring. The presence of C-rich PAH grains is even more remarkable in an oxygen dominated chemistry. However, it should be noted that PAH emission is observed in some RSG (Sylvester et al. 1999) demonstrating that C-rich PAHs can form in an O-rich environment. In these sources there is no hot, fast wind to interact with the silicate dust. The UV-photons needed to excite the PAH molecules in this case are expected to come from a warm chromosphere.

8.2. morphology of the dusty nebulae

The geometry of the dust shells around Wra 751 and AG Car show a number of similarities: both are elongated (AG Car more so than Wra 751), with a bipolar dust brightness distribution along the minor axis. A similar morphology of the dust is also seen in HD 168625 (Skinner 1997; Robberto & Herbst 1998), a low luminosity LBV (Hutsemékers et al. 1994), though the total dust mass in this dust shell is much lower (10^{-4} – $3{\times}10^{-3}$ $M_\odot$ yr^{-1}). The stellar luminosity of Wra 751 is at or below the Humphreys-Davidson (HD) limit and therefore this star may very well have been a RSG when it produced its dust shell. The similarity of the nebular morphology between AG Car and Wra 751 may point to a similar formation history.

Apart from the similarities there is also an important difference in morphology between Wra 751 and AG Car. In the latter case, ionized gas and dust are co-spatial, while for Wra 751 the bulk of the dust is outside the ionized region. This difference can be explained if we assume that the Wra 751 nebula is younger than the AG Car nebula, i.e. the ionization of the envelope has only recently started in Wra 751. We note that the derived ionized mass for Wra 751 of 3.2 $M_\odot$ (HvD) is somewhat high for this scenario, however, this value is uncertain.

Our dust models indicate that the bulk of the emission near 10 μm is probably caused by small grains. Therefore, the 10 μm ground-based images presented in Sect. 6 allow us to determine the location of these grains. At the same time, these images may be somewhat misleading since the spatial distribution of small and large grains need not necessarily be the same, and the bulk of the dust mass may be distributed differently from what we see at 10 μm. A different distribution of small and large grains could be investigated by obtaining images at longer wavelengths. Unfortunately, the spatial extent of the Wra 751 and AG Car nebulae is too small to be resolved by IRAS, and to our knowledge there were no observations done with ISOPHOT to study the spatial extent of the dust at longer wavelengths.

Several WR ring nebulae, however, are large enough to study with IRAS data (e.g. Marston 1996; van Buren & McCray 1998; Mathis et al. 1992). Their morphology is very similar to that of AG Car and Wra 751, though they are usually much larger. To indicate the morphological similarities between these nebulae, we show high resolution IRAS images, using the HIRAS image reconstruction package (Bontekoe et al. 1994) of the nebula surrounding WR 40, RCW 58, at 25 and 60 μm (Fig. 11). Since this nebula is larger than the two nebulae studied in this paper, dust temperatures are much lower, and the presence of the dusty nebula is not very clear at 12 μm. It is immediately clear that at 25 and 60 μm the nebula has similar shape and size. In a

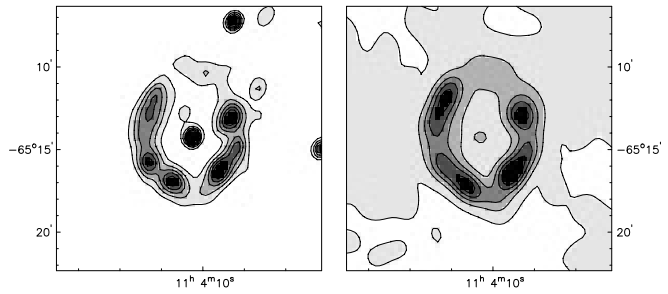

Fig. 11. 25 and 60 μm HIRAS images of the nebula RCW 58 around WR 40. Contours are drawn each 0.8 (at 25 μm) and 5 MJy/sr (at 60 μm), respectively, with the lowest contour at 1.5 MJy/sr. The diameter of the nebula is approximately 5 arcmin. The 25 μm image is partly due to very small warm dust grains, the 60 μm image mainly to larger, cold grains. The identical morphology indicates that also the small grains are located in the ring nebula.

detailed study of the infrared properties of WR ring nebulae, Mathis et al. (1992) conclude that for RCW 58 "the emission in the IRAS 25 μm filter must be contributed by transient heating of small grains or emission from molecules excited by absorption of a single photon". The similarity of the 25 and 60 μm images indicates that these grains are located in the ring nebula. We have compared the dust and Hα morphology of RCW 58, using our HIRAS images and the Hα image published by Marston (1995), and found excellent agreement, i.e. the ionized gas and dust are co-spatial.

Another similarity between the nebulae of LBVs and WR stars comes from recent very high-resolution HST images of M1-67 (Grosdidier et al. 1998). They show that this nebula, which surrounds the Wolf-Rayet star WR 124, contains numerous bright unresolved knots of emission, often surrounded by what appear to be their local "wind" diffuse bubbles. The nebula of AG Car contains similar pockets of emission (Nota et al. 1995), which are explained as the result of a *non-linear thin shell instability* (Vishniac 1994), producing a shock which in turn generates the "cometary tails" seen in the images. This instability is possibly caused by the interaction of the LBV wind with a previous slower wind.

Thus, a possible evolutionary link between the nebulae of LBVs and WR stars is suggested by (**a**) the presence of a population of small non-TE grains, (**b**) their location in the ring nebula (together with the colder dust particles in TE) and (**c**) the detailed morphological structure of the nebulae.

8.3. central star

There are significant differences between the two central objects. The most notable difference is their stellar luminosity: AG Car has a luminosity equal to or larger than $10^{6.0}$ $L_\odot$ (Lamers et al. 1989; Leitherer et al. 1994) whereas Wra 751 probably has a luminosity of the order of $10^{5.7}$ $L_\odot$ (Hu et al. 1990). Another difference is the more pronounced photometric and spectroscopic variability of AG Car, though the average effective temperatures are very similar. Also, the central stars have rather different present-day stellar winds, with a mass-loss rate for Wra 751 (10^{-6} $M_\odot$ yr^{-1}, Hu et al. 1990) about two orders of magnitude lower than that of AG Car (10^{-4} $M_\odot$ yr^{-1}, Leitherer et al. 1994).

8.4. Evolutionary considerations

So, were AG Car and Wra 751 red supergiants when they produced their dust shells? Despite the observed lack of cool stars with luminosities above log ($L/L_\odot$) = 5.8, AG Car has often been suggested to have been a red supergiant when producing its circumstellar dust shell (e.g. Viotti et al. 1988, McGregor et al. 1988). Recent evidence in support of this view comes from nebular abundance determinations (Smith et al. 1997). Our analysis of the composition of the dust in Wra 751 and AG Car, as well as the nebular morphology, clearly suggest a high degree of similarity in the formation history of the nebulae. This is of importance because AG Car is above the HD limit, while Wra 751 is not. The shell around Wra 751 therefore could have been produced in a RSG phase.

The dust composition also links the LBVs to RSGs: in both classes of objects crystalline pyroxenes condense, and evidence is accumulating that these grains only condense in high-density outflows. Voors et al. (1999) show that the LBV R71 in the LMC has crystalline olivines that strongly resemble those in the galactic RSG NML Cyg. We point out however that, while AG Car and Wra 751 show crystalline pyroxenes and little evidence for olivines, the RSG show both crystalline olivines and pyroxenes, reflecting some differences in the dust condensation conditions.

Another link between LBVs and RSGs is the derived time-averaged mass-loss. Present-day dust mass-loss rates of RSGs are on the order of a few times 10^{-6} $M_\odot$ yr^{-1} (e.g. Jura 1996). This agrees well with the derived time-averaged mass-loss rate of Wra 751, whereas that of AG Car is about a factor of ten higher. The luminosity of Wra 751 is similar to that of the most luminous RSGs, whereas that of AG Car is much higher. This suggests that a relation may exist between the time-averaged mass-loss rate during the RSG phase and the stellar luminosity.

The detection of an inner, unresolved shell in Wra 751 which probably also contains dust indicates that the mass-loss history of this star may have been more complex than previously assumed. It is possible that, while the dusty envelope was produced in a phase of very high mass loss, this phase was followed by (a) shorter period(s) of enhanced mass loss and dust formation. Alternatively, the entire dust shell may have been produced by subsequent short bursts of high mass loss, much like the scenario proposed by Nota et al. (1995), but in that case the dust formation conditions are not necessarily similar to those in RSG.

The high mass-loss phase for both Wra 751 and AG Car lasted about 6000 years (see Sect. 7.3). However, we stress that the derived outer radii of the dust shells are difficult to constrain. Nevertheless, these time-scales may be difficult to reconcile with the observed lack of luminous RSG in the HR diagram, given the number of blue stars at high luminosity. It is possible that observational selection effects play a role, since a star with such a high dusty mass loss would be heavily obscured at optical

Table 3. Dust shell parameters

	R_{in} (pc)	R_{out} (pc)	a_{min} (μm)	a_{max} (μm)	M_{dust} ($M_\odot$)	$\overline{\dot{M}}$ ($M_\odot$ yr^{-1})	τ_{shell} (yrs)
Wra 751	0.17	0.34	0.03	1	1.7×10^{-2}	2.7×10^{-6}	6.3×10^{3}
AG Car	0.37	0.80	0.25	40	2.5×10^{-1}	3.4×10^{-5}	6.0×10^{3}

and UV wavelengths, and thus escape detection when optical search methods are used. The IRAS all-sky survey would have revealed such IR-bright objects in our galaxy (it would rival η Car in IR brightness) but none have been identified. Perhaps not all stars with masses above 50 $M_\odot$ go through a dusty mass loss phase. For instance, P Cygni and S Dor are examples of LBVs without massive dusty ring nebula. Marston (1996) finds that about 60 percent of galactic WR stars have dusty ring nebulae. This also suggests that perhaps not all massive stars form dusty ring nebulae shortly before they enter the WR phase.

The duration of the LBV phase can be estimated in a number of different ways. If one assumes that on average an LBV has to lose 10 $M_\odot$ and does so with an average mass-loss rate of 10^{-4} $M_\odot$ yr^{-1}, then the LBV phase will last approximately 10^5 years. There is, however, a large uncertainty in the average mass-loss rate. The mass lost during outburst may significantly (factor of 10) increase the average mass-loss rate and hence lower the lifetime of the LBV phase. From statistical arguments, by comparing the number of LBVs to the number of WR stars, Lamers (1989) estimates an LBV lifetime between 5×10^3 and 5×10^4 years. Based on the same statistical arguments, Humphreys & Davidson (1994) give $\tau_{\rm LBV} \sim 2.5 \times 10^4$ years, but note that this may be an underestimate. It is clear that the derived average lifetime for LBVs depends critically on the definition of an LBV. There is a large group of "candidate" LBVs, and if these are included the sample of LBVs becomes much larger, which would increase the derived LBV lifetime.

It is important to distinguish two classes of LBVs; those above and those below the HD-limit. Usually, in discussing the statistics of LBVs this distinction is not explicitly made. Let us first look at the LBVs with dusty envelopes *below* the HD limit (e.g. HR Car). These stars likely were RSG when they produced the dust shell. Evolutionary tracks show that the luminosity of massive stars is roughly constant when they evolve off the main sequence to the red. Therefore, such objects remain below the HD limit throughout their entire post-main-sequence life. Thus, LBVs below the HD limit should not be counted when discussing the lack of stars in the upper right of the HRD.

There are *very few* LBVs above the HD limit with dusty envelopes: in our galaxy, AG Car and η Car are well established, while in the LMC R127 (and possibly R143) is found above the HD limit. The formation history of the η Car ejecta is likely very different from those of the other LBVs (cf. the dynamics, the nebular abundances and the dust composition), and should not be included in these statistics. Thus, the probability of catching a star above the HD limit in the process of ejecting a dusty envelope is small. This significantly alleviates the apparent discrepancy between the observed number of dusty LBVs and the lack of luminous RSG above the HD limit.

9. Conclusions

In this paper we have presented infrared imaging and spectroscopy of Wra 751 and AG Car. The individual conclusions that we reach, separated in similarities and differences between the two objects, are shown in Table 2.

Using a 1-D radiative transfer code, and assuming the dust to consist of amorphous pyroxenes, we have determine a number of parameters for the dust shells of Wra 751 and AG Car. These are given in Table 3.

Specific points concerning the evolution of the two objects, as a result of studying the two nebulae are the following:

1. Based on the similarities between the nebulae of AG Car and Wra 751 (morphology, particle size [to some extent] and grain type) we suggest that they may have had similar formation histories.
2. Similarities in the dust between Wra 751 and AG Car on the one hand and RSGs on the other, suggest that the nebulae around the LBVs may have been formed during a RSG phase.
3. The time-averaged mass-loss rates of Wra 751 and AG Car are consistent with a previous RSG phase.
4. Similarities between the two nebulae studied in this paper and WR ring nebulae also suggests an evolutionary connection: LBV nebulae may be the precursors of WR ring nebulae.
5. We present several pieces of evidence which, taken together, lead us to assume that for both objects the present-day dusty shells may well have been formed during a stage in which they were cool supergiants. Taken by themselves, however, these pieces of evidence are not conclusive.

Acknowledgements. LBFMW and AdK acknowledge financial support from an NWO *Pionier* grant. AdK is also grateful for support from NWO *Spinoza* grant 08-0 to E.P.J. van den Heuvel. We thank P.A. Zaal for providing the sub-millimeter observation of AG Car. We thank T.L. Lim for reducing the LWS spectra of Wra 751 and AG Car. The IRAS data were obtained using the IRAS data base server of the Space Research Organisation of the Netherlands (SRON) and the Dutch Expertise Centre for Astronomical Data Processing funded by NWO. We thank the referee for valuable comments and suggestions.

References

Allen D.A., Jones T.J., Hyland A.R., 1985, ApJ 291, 280
Andriesse C.D., Donn B.D., Viotti R., 1978, MNRAS 185, 771
Bertie J.E., Labbé H.J., Whalley E., et al., 1969, JChPh 50, 4501
Bontekoe Tj.R., Koper E., Kester D.J.M., 1994, A&A 284, 1037
Clegg P.E., Ade P.A.R., Armand C., et al., 1996, A&A 351, L38
de Graauw Th., Haser L.N., Beintema D.A., et al., 1996, A&A 315, L49

de Jager C., van Genderen A.M., 1989, In: Davidson K., Moffat A., Lamers H. (eds.), Physics of Luminous Blue Variables, IAU Colloquium 113, p.127
de Koter A., Schmutz W., Lamers H.J.G.L.M., 1993, A&A 277, 561
de Koter A., Heap S.R., Hubeny I., 1997, ApJ 477, 792
de Winter D., Perez M.R., Hu J.Y., Thé P.S., 1992, A&A 257, 632
Garcia-Lario P., Riera A., Manchado A., 1998, A&A 334, 1007
Grosdidier Y., Moffat A.F.J., Joncas G., et al., 1998, ApJ 506, L127
Hu J.Y., de Winter D., Thé P.S.,Perez M.R., 1990, A&A 227, L17
Humphreys R.M., Davidson K., 1979, ApJ 232, 409
Humphreys R.M., Davidson K., 1994, PASP 106, 1025
Humphreys R.M., Jones T.J., Gherz R.D., 1987, AJ 94, 315
Humphreys R.M., Lamers H.J.G.L.M., Hoekzema N., et al., 1989, A&A 218, L17
Hutsemékers D., 1997, In: A. Nota, H. Lamers (eds.), Luminous Blue Variables: Massive Stars in Transition, ASP Conference series vol. 120, p. 316
Hyland A.R., Robinson G., Mitchell R.M., et al., 1979, ApJ 233, 145
Hutsemékers D., 1994, A&A 281, L81
Hutsemékers D., van Drom E., 1991, A&A 251, 620
Hutsemékers D., van Drom E., Gosset E., Melnick J., 1994, A&A 290, 906
Jäger C., Molster F.J., Dorschne J., et al., 1998, A&A 339, 904
Jura M., 1996, ApJ 472, 806
Käufl H.U., Juoan R., Lagage P.O., et al., 1994, Infrared Phys. Tech. 35, 203
Kessler M.F., Steinz J.A., Anderegg M.E., et al., 1996, A&A 315, L27
Koike C., Shibai H., Tuchiyama A., 1993, MNRAS 264, 654
Kurucz R.L., 1991, In: L. Crivellari, I. Hubeny, D.G. Hummer (eds.), Stellar Atmospheres–Beyond Classical Models, NATA ASI Series, series C, vol. 341, p. 441
Lamers H.J.G.L.M., 1989, In: K. Davidson, A. Moffat, H. Lamers (eds.), Physics of Luminous Blue Variables, IAU Colloquium 113, p. 135
Lamers H.J.G.L.M., Hoekzema N., Trams N.R., et al., 1989, In: K. Davidson, A. Moffat, H. Lamers (eds.), Physics of Luminous Blue Variables, IAU Colloquium 113, p. 271
Lamers H.J.G.L.M., de Groot M.J.H., 1992, A&A 257, 153
Lamers H.J.G.L.M., Morris P.W., Voors R.H.M., et al., 1996, A&A 315, 225
Léger A., Puget J.L., 1984, A&A 137, L5
Leitherer C., Allen R., Altner B., et al., 1994, ApJ 428, 292
Lemke D., Klaas U., Abolins J., et al., 1996, A&A 315, L64
Marston A.P., 1995, AJ 109, 1839
Marston A.P., 1996, AJ 112, 2828
Marston A.P., Nota A., Pasquali A., et al., 1999, Variable and Non-spherical Stellar Winds in Luminous Hot Stars, IAU Colloquium 169, B. Wolf, A. Fullerton, O. Stahl (eds.)
Mathis J.S., Rumpl W., Nordsieck K.H., 1977, ApJ 217, 425
Mathis J.S., Cassinelli J.P., van der Hucht K.A., et al., 1992, ApJ 384, 197
McGregor P.J., Finlayson K., Hyland A.R., 1988, ApJ 329, 874
Meynet G., Maeder A., Schaller G., et al., 1994, A&AS 103, 97
Neugebauer G., Habing H.J., van Duinen R., et al., 1984, ApJL 278, L1
Nota A., Leitherer C., Clampin M., et al., 1992, ApJ 398, 621
Nota A., Livio M., Clampin M., Schulte-Ladbeck R., 1995, ApJ 448, 788
Robberto M., Herbst T.M., 1998, ApJ 498, 400
Robinson G., Mitchell R.M., Aitken D.K., et al. 1987, MNRAS 227, 535
Rogers C., Martin P.G., Crabtree D.R., 1983, ApJ 272, 175
Seab C.G., Snow T.P., 1989, ApJ 347, 479
Savage B.D., Mathis J.S., 1979, ARAA 17, 73
Shore S.N., Altner B., Waxin I., 1996, AJ 112, 2744
Skinner C.J., 1997, in: Luminous Blue Variables: Massive Stars in Transition, A. Nota, H. Lamers (eds.), ASP Conference series, vol. 120, p. 322
Smith L.J., 1991, In: K. van der Hucht, B. Hidayat (eds.), Wolf-Rayet stars and interrelations with other massive stars in galaxies, IAU Symposium 143, p. 385
Smith L.J., 1997, In: A. Nota, H. Lamers (eds.), Luminous Blue Variables: Massive Stars in Transition, ASP Conference series, vol. 120, p. 310
Smith C.H., Aitken D.K., Moore T.J.Y., et al., 1995, MNRAS 273, 354
Smith L.J., Stroud M.P., Esteban C., Vilchez J.M., 1997, MNRAS 290, 265
Smith L.J., Nota A., Pasquali A., et al., 1998, ApJ 503, 278
Smith N., Gehrz R.D., Krautter J., 1998, AJ 116, 1332
Spoon H.W.W., de Koter A., Sterken C., et al., 1994, A&AS 106, 141
Stahl O., 1986, A&A 164, 321
Stahl O., 1997, In: A. Nota, H. Lamers (eds.), Luminous Blue Variables: Massive Stars in Transition, ASP Conference series, vol. 120, p. 100
Sylvester R.J., Skinner C.J., Barlow M.J., 1999, MNRAS 301, 1083
Thackeray A.D., 1950, MNRAS 110, 526
Thackeray A.D., 1977, MNRAS 180, 95
Trams N.R., van Tuyll C.I., Voors R.H.M., et al., 1999, In: B. Wolf, A. Fullerton, O. Stahl (eds.), Variable and Non-spherical Stellar Winds in Luminous Hot Stars, IAU Colloquium 169
van Buren D., McCray R., 1998, ApJ 329, L93
van Genderen A.M., Thé P.S., 1985, Sp.Sc.Rev. 39, 317
van Genderen A.M., Thé P.S., de Winter D. et al., 1992, A&A 258, 316
Viotti R., Cassatella A., Ponz D., Thé P.S., 1988, A&A 190, 333
Vishniac E.T., 1994, ApJ 428, 186
Voors R.H.M., Waters L.B.F.M., Trams N.R., Käufl H.U., 1997, A&A 321, L21
Voors R.H.M., Waters L.B.F.M., Morris P.W., Trams N.R., et al., 1999, A&A 341, L67
Voors R.H.M., 1999, Ph.D thesis, Utrecht University
Waters L.B.F.M., Wesselius P.R., 1986, A&A 155, 104
Waters, L.B.F.M., Morris, P.W., Voors, R.H.M., et al., 1997, In: A. Nota, H. Lamers (eds.), Luminous Blue Variables: Massive Stars in Transition, ASP Conference series, vol. 120, p. 326